Heineke, C., Niedermann, S., Hetzel, R., Akal, C. (2016): Surface exposure dating of Holocene basalt flows and cinder cones in the Kula volcanic field (Western Turkey) using cosmogenic 3He and 10Be. - *Quaternary Geochronology*, *34*, pp. 81—91.

DOI: http://doi.org/10.1016/j.quageo.2016.04.004

Surface exposure dating of Holocene basalt flows and cinder cones in the Kula volcanic field (Western Turkey) using cosmogenic ^{3}He and ^{10}Be

Caroline Heineke [a*], Samuel Niedermann [b], Ralf Hetzel [a], Cüneyt Akal [c]

[a] Institut für Geologie und Paläontologie, Westfälische Wilhelms-Universität Münster, Corrensstr. 24, D-48149 Münster, Germany

[b] Helmholtz-Zentrum Potsdam – Deutsches GeoForschungsZentrum (GFZ), Telegrafenberg, D-14473 Potsdam, Germany

[c] Dokuz Eylül University, Engineering Faculty, Department of Geological Engineering, Tınaztepe Campus, Buca, TR-35160 Izmir, Turkey

[*] Corresponding author, caroline.heineke@uni-muenster.de, Phone: +49 (0) 251 83-33936, Fax: +49 (0) 251 83-33933

Abstract

The Kula volcanic field in Western Turkey comprises about 80 cinder cones and associated basaltic lava flows of Quaternary age. Based on geomorphological criteria and K-Ar dating, three eruption phases, β2–β4, were distinguished in previous studies. Human footprints in ash deposits document that the early inhabitants of Anatolia were affected by the volcanic eruptions, but the age of the footprints has been poorly constrained. Here we use ^{3}He and ^{10}Be exposure dating of olivine phenocrysts and quartz-bearing xenoliths to determine the age of the youngest lava flows and cinder cones. In the western part of the volcanic field, two basalt samples from a 15-km-long block lava flow yielded ^{3}He ages of 1.5±0.3 ka and 2.5±0.4 ka, respectively, with the latter being in good agreement with a ^{10}Be age of 2.4±0.3 ka for an augen gneiss xenolith from the same flow. A few kilometers farther north, a metasedimentary xenolith from the top of the cinder cone *Çakallar Tepe* gave a ^{10}Be age of 11.2±1.1 ka, which dates the last eruption of this cone and also the human footprints in the related ash deposits. In the center of the volcanic field, a basalt sample and a metasedimentary xenolith from another cinder cone gave consistent ^{3}He and ^{10}Be ages of 2.6±0.4 ka and 2.6±0.3 ka, respectively. Two β4 lava flows in the central and eastern part of the volcanic province yielded ^{3}He ages of 3.3±0.4 ka and 0.9±0.2 ka, respectively. Finally, a relatively well-preserved β3 flow gave a ^{3}He age of ~13 ka. Taken together, our results demonstrate that the penultimate eruption phase β3 in the Kula volcanic field continued until ~11 ka, whereas the youngest phase β4 started less than four thousand years ago and may continue in the future.

Keywords: lava flow, cosmogenic ^{10}Be, cosmogenic ^{3}He, Kula volcanic field, Turkey

1. Introduction

Dating of Quaternary volcanic rocks is essential to decipher the recent eruption history of large volcanoes or volcanic provinces and to assess the associated hazards. The huge impact of major volcanic eruptions on human cultures and societies was already perceived in Paleolithic times, as illustrated by ~35-ka-old paintings in the Chauvet-Pont d'Arc cave (Ardèche, France), which show a strombolian volcanic eruption and are similar in age to volcanic rocks in the nearby Bas-Vivarais region (Nomade et al., 2016). Another example from Neolithic time is provided by a wall painting with a ^{14}C age of ~6600 BC, which depicts the eruption of a twin volcano in Central Anatolia that occurred around the same time as constrained by (U-Th)/He dating (Schmitt et al., 2014). Much later, the eyewitness *Pliny the Younger* described the catastrophic eruption of the Vesuvius, which led to the destruction of Pompeii in 79 AD. Already a hundred years earlier, in ~20 BC, the Greek historian and geographer Strabo gave one of the first written accounts on a volcanic province, which he described as "Katakekaumene" ("burned lands"). Strabo emphasized the fertility of its soils and the suitability of the volcanic ash deposits for viticulture (Radt, 2004; Akdeniz, 2011). Today, this volcanic province is known as the Kula volcanic field in Western Turkey (Fig. 1).

The presence of well-preserved footprints in the ash deposits of the cinder cone *Çakallar Tepe* demonstrates that the humans inhabiting Western Anatolia were affected by volcanic eruptions that occurred in the Kula volcanic field (e.g. Ozansoy, 1969; Barnaby, 1975; Tekkaya, 1976; Kayan, 1992; Akdeniz, 2011). The age of the footprints has been much disputed. Initially, an age of ~250 ka was suggested by Ozansoy (1969) based on a spurious correlation with sediments for which he assumed a deposition during the Mindel glacial stage – an approach that was strongly criticized by Tekkaya (1976). Ercan et al. (1985) used a K-Ar age of 25±6 ka for basalts from a different cone more than ten kilometers away as age constraint for the footprints, which is highly questionable as well. Finally, a thermoluminescence (TL) age of 49±9 ka for orthoclase and hornblende crystals scraped from one footprint was reported by Göksu (1978) along with a younger TL age of 26±5 ka for the overlying scoria deposits. However, the large age gap renders the two TL ages doubtful, because the geological context indicates that the deposition of the tuff, the imprinting of the footprints, and their burial by scoria occurred in quick succession during the same eruption cycle (Barnaby, 1975; Westaway et al., 2004). In conclusion, reliable age data for the last eruption of *Çakallar Tepe* and, by inference, the footprints are still lacking.

The volcanic rocks of the Kula volcanic field were initially subdivided into four different groups (β1–β4) on the basis of geomorphological criteria (Fig. 2; Hamilton and Strickland, 1841; Canet and Jaoul, 1946). The oldest group, β1, was subsequently abandoned, because field observations revealed that the β1 basalts at a key locality are actually slope deposits that contain clasts of β3 lava (Richardson-Bunbury, 1996). The oldest eruption phase β2 occurred between ~1.3 Ma and ~0.9 Ma, as shown by several K-Ar ages obtained from whole rock samples (including phenocrysts) and samples of ground mass (Borsi et al., 1972; Westaway et al., 2004 and 2006). K-Ar ages for lava flows of the subsequent β3 phase range from ~240 ka to ~80 ka (Westaway et al., 2004 and 2006), whereas volcanic rocks attributed to the final β4 phase yielded ages between 74±15 ka and 11±5 ka (Ercan et al., 1985; Westaway et al., 2004). However, the relatively old ages for basalts of the β4 group are difficult to reconcile with the pristine appearance of the respective lava flows and cinder cones in the field. As discussed by Westaway et al. (2004), the presence of small amounts of excess argon in the ground mass of the dated basalts has likely caused an overestimation of the eruption ages. The problem of excess argon is even worse for amphibole phenocrysts, as shown by the $^{40}Ar/^{39}Ar$ ages of Paton (1992), most of which were interpreted as unreliable by Westaway et al. (2004). By paying particular attention to the careful characterization and preparation of fresh, fine-grained groundmass samples, a subsequent study obtained K-Ar ages of 7±2 ka and 4±2 ka for two β4 basalt samples, while two other samples did not contain any measurable amounts of radiogenic ^{40}Ar and provided a zero age (Westaway et al., 2006). That study indicates that the β4 basalts formed during the Holocene, although their age is still not well constrained.

Surface exposure dating using *in situ*-produced cosmogenic nuclides offers the possibility to determine reliable ages for volcanic rocks, in particular for young lava flows that have not been significantly eroded (e.g. Craig and Poreda 1986; Laughlin et al., 1994; Ammon et al., 2009; Foeken et al., 2009; Marchetti et al., 2014). In this study, we present the first cosmogenic ^{3}He ages (n = 7) for olivine from basalt samples of young lava flows and cinder cones of the Kula volcanic field. These are complemented by three ^{10}Be exposure ages for quartz-bearing xenoliths, which we discovered in tuff deposits of two cinder cones and one basaltic lava flow.

2. Geological setting and geomorphology of the volcanic deposits

Tertiary and Quaternary volcanic rocks cover considerable parts of Western Turkey, a region that belongs to the backarc of the Hellenic subduction zone (Fig. 1a). The southward-younging of the volcanic rocks has been attributed to the rollback of the subducting African plate (e.g. Fytikas et al., 1984; Innocenti et al., 2005), a process that also caused considerable crustal extension in the upper plate (e.g. Faccenna et al., 2003; Brun and Sokoutis, 2010) and thinning of its mantle lithosphere (Alıcı et al., 2002; Prelević et al., 2012). In Western Turkey, the ongoing NNE-SSW directed extension commenced in the Late Oligocene/Early Miocene and has led to the exhumation of mid-crustal metamorphic rocks in the Menderes Massif by detachment-faulting, normal faulting, and erosion (e.g. Thomson and Ring, 2006; Glodny and Hetzel, 2007; Buscher et al., 2013), and also to the formation of several E-W-trending grabens (e.g. Seyitoğlu and Scott, 1991; Bozkurt, 2000; Purvis and Robertson, 2004). The two largest of these grabens – the Büyük Menderes and the Gediz graben (Fig. 1a) – divide the Menderes Massif into a southern, a central, and a northern submassif.

The Kula volcanic field in the northern Menderes submassif is the youngest volcanic field in Western Turkey and located about 20 km north of the Gediz graben (Fig. 1b). The volcanic deposits around Kula comprise about 80 basaltic cinder cones, which consist mainly of scoria, basaltic lava flows (i.e. alkali olivine basalts, basanites, and phonotephrites), and minor tuff and tephra deposits (e.g. Richardson-Bunbury, 1996; Güleç, 1991; Alıcı et al., 2002; Şen et al., 2014 and references therein). The Na-dominated OIB-like magmas were derived from the convecting asthenospheric mantle and suffered only minor crustal contamination (e.g. Prelević et al., 2012). Note that the cinder cones from which these magmas erupted are commonly named *Tepe*, although the Turkish word *Tepe* means hill and does not explicitly refer to volcanic cones.

The three different groups of Quaternary volcanic rocks (β2–β4) in the Kula volcanic field have distinct geomorphological characteristics. In the eastern part of the volcanic field, 1.3–0.9 Ma-old β2 lava flows that overlie fluvial sand and gravel deposits form plateaus at an elevation of ~580–600 m (Fig. 2). The Gediz River has incised these flows by 150–200 m and formed a sequence of fluvial terraces that record the surface uplift of the entire region (e.g. Westaway et al., 2006; Maddy et al., 2012). The younger β3 lava flows, which cover the largest area of the volcanic field (Fig. 2), occur only 25–40 m above the Gediz River and its tributaries (Hamilton and Strickland, 1841; Westaway et al., 2006). These younger flows are typically covered by well-developed soils and used for agriculture. The Holocene β4 lavas form three major block lava flows (Fig. 2) that locally cascade downslope to the present course of the Gediz River (Westaway et al., 2006). These basalt flows show no signs of soil development and are largely unvegetated, although a few small bushes do locally occur. The mean thickness of the flows is ~10 m and commonly they have a local relief of several meters (Richardson-Bunbury, 1996). Although smooth surfaces with flow features are locally preserved, the morphology of the β4 flows is dominated by sharp-edged basalt boulders ranging from a few decimeters up to several meters in size. Boulder surfaces are often glassy and exhibit a vesicular texture in the uppermost 10–20 cm, indicating no or negligible surface erosion. Commonly, the angular boulders are draped by a thin cover of lichen and moss. The β4 basalts contain large (up to 5 mm) olivine phenocrysts and in some places also amphibole phenocrysts (e.g. Güleç, 1991; Westaway et al., 2004).

3. Sampling

For exposure dating of the most recent eruption phase (β4) of the Kula volcanic field, we collected six basalt samples for ^{3}He dating of olivine and two quartz-bearing xenoliths for ^{10}Be dating of quartz (Table 1). Three of the six basalt samples were collected in the western part of the volcanic field from a 15-km long block lava flow, which originated from the *Divlit Tepe* cinder cone and flowed in southwesterly direction (Fig. 2). Two of these samples (13T2 and 13T3) were taken north of Adala village near the end of the flow from two basalt blocks with a size of ~0.8 and ~1.5 m, respectively. In the vicinity of these samples, we discovered an angular, 9-cm-thick block of augen gneiss at the surface of the lava flow (Fig. 3a). The rectangular gneiss block, which we collected as a whole (sample 13T4), was tightly coalesced to a block of basalt lava underneath it. Another basalt sample (13T14) from the same flow was taken ~2 km downstream of the Demirköprü dam (Fig. 2) from a smooth lava flow surface with a wavy texture (Fig. 3b).

In the central part of the volcanic field, we collected one basalt sample near the center of a large lava flow (Fig. 2). This sample (13T7) was taken from the top of a huge block that has exceptionally well preserved flow features (Fig. 3c). The sampled surface is slightly convex and has a dip of 12° at the sampling spot. About three kilometers farther southeast (near Sandal village), we collected one basalt sample and one quartz-bearing xenolith from a small cinder cone. The metasedimentary xenolith (13T5) was found at the outer rim of the small crater located at the top of the cone. The xenolith had a rounded shape and was firmly attached to basaltic lava and welded tuff deposits underneath (Fig. 3d). The basalt sample (13T6) was collected from the subhorizontal surface of a large basalt block on the upper slope of the cone (Fig. 3e).

The last basalt sample from a β4 lava flow (13T9) was taken ~5 km north of Kula in the eastern part of the volcanic field (Fig. 2). The sample stems from a relatively smooth surface (4 x 5 m) with a dip of 10°, which is located close to the margin of the otherwise irregular block lava flow. The sampled surface shows several steps with a height of a few centimeters that are oriented perpendicular to the flow direction of the lava. The presence of thin soil (≤3 cm) along these steps may indicate a small amount of erosion of the entire surface, which we estimated as ~2 cm in the field.

In addition to the samples from β4 lavas described above, we took one sample from a β3 lava flow and another sample from the cinder cone *Çakallar Tepe*. This cone is of particular interest because in the basal ash, which was deposited during its last eruption, fossil human footprints were discovered during the construction of the Demirköprü dam in 1969 (Fig. 3f) (e.g. Ozansoy, 1969; Barnaby, 1975). The footprints occur ~500 m west of the cone and were protected from erosion by scoria deposits that cover its flanks and the areas south and west of the cone. As the volcanic deposits of the cinder cone do not contain olivine phenocrysts and can therefore not be dated with ^{3}He, we used a fine-grained metasedimentary xenolith discovered at the top of the cone for ^{10}Be dating (13T15). The round xenolith with a diameter of ~20 cm was partly exposed, but firmly embedded in the coarse volcanic tuff deposits of the outer crater rim.

The basalt sample 13T12 was taken from a small β3 lava flow near Yeniköy village in the eastern part of the volcanic field (Fig. 2). The sampling site exhibits a smooth flow surface sparsely covered by grass and soil with a thickness of up to two centimeters. Sampling was carried out on an unvegetated patch of this surface. Based on the presence of vesicles, which commonly occur in the uppermost decimeters of lava flows, we estimate that no more than 10±5 cm of material was eroded from the sampled surface.

4. Density determination, mineral separation and analytical procedures

4.1 Density determination

For calculating surface exposure ages, the density of rock samples must either be assumed or measured. We determined the bulk density of four basalt samples and the three quartz-bearing xenoliths by weighing the samples in air and in water (Balco and Stone, 2003). The bulk density ρ was calculated as:

$$\rho = m_a \rho_w / (m_a - m_w) \qquad (1)$$

where m_a (g) is the sample weight in air, m_w (g) is the weight of the sample immersed in water, and ρ_w (g cm^{-3}) is the water density. The basalt samples yielded similar densities with a mean of 2.3 g cm^{-3}. The density of the three xenoliths was more variable, with values of 2.1 g cm^{-3} (13T4), 2.5 g cm^{-3} (13T5), and 2.3 g cm^{-3} (13T15) (Table 1).

4.2 Preparation of olivine and quartz samples and chemical separation of Be

The separation of olivine and quartz and the chemical separation of Be from the quartz samples was carried out at the cosmogenic nuclide laboratory of the University of Münster. All basalt and xenolith samples were crushed, sieved, and washed. The 500–1000 µm grain size fraction of the basalt samples was then split into a magnetic, matrix-dominated and a less-magnetic, olivine-rich fraction using a Frantz magnetic separator. Olivine was separated from the enriched 500–1000 µm fraction by hand-picking under a binocular, considering limpid, non-altered, and predominantly inclusion-free crystals only. Finally, the olivine samples were etched in aqua regia at 40 °C in an ultrasonic bath for 1–2 hours to remove iron oxides and matrix adhesions.

To separate quartz from the three xenolith samples, we used the 250–500 µm grain size fractions of samples 13T4 and 13T5, and the 63–125 µm size fraction from the fine-grained sample 13T15. As the augen gneiss xenolith yielded enough material for the preparation of two quartz samples, we prepared and analyzed two aliquots (i.e. 13T4a,b). The grain size fractions were split into a magnetic and a non-magnetic fraction. The subsequent leaching procedure consisted of one etching step in 6 M HCl at 80 °C, four subsequent etching steps in dilute HF/HNO_3 in a heated ultrasonic bath (Kohl and Nishiizumi, 1992), and two alternating etching steps in aqua regia and 8 M HF to obtain pure quartz (Goethals et al., 2009). For beryllium extraction, ~0.3 mg of Be carrier with a $^{10}Be/^{9}Be$ ratio of $2.2\pm0.6 \times 10^{-15}$ was added to each sample. Following complete dissolution of quartz in HF (40 %), the samples were redissolved and converted into chloride form using 6 M HCl. Beryllium was separated using successive anion and cation exchange columns and precipitated as $Be(OH)_2$ at pH 8–9. Following the transformation to BeO at 1000 °C and target preparation, ^{10}Be was analyzed at the accelerator mass spectrometer facility of ETH Zurich (Christl et al., 2013).

4.3 Helium analysis and correction for radiogenic ^{4}He and nucleogenic ^{3}He

All analytical procedures required for ^{3}He exposure dating were performed at the noble gas laboratory of the German Research Centre for Geosciences (GFZ). First, all olivine separates were crushed in vacuo by squeezing between two hard-metal plates to release and measure magmatic helium trapped in melt and fluid inclusions. Subsequently, the material retrieved from the crusher was wrapped in Al foil and placed in the sample carrousel above the extraction furnace, which was baked at 100°C for one week. After dropping them into the tantalum crucible, samples were heated to 1750 °C to extract and analyze the helium remaining after crushing.

After gas extraction by either crushing or heating, chemically active gases were removed in Ti sponge and SAES (ZrAl) getters, and the noble gases were adsorbed to activated charcoal in a cryogenic adsorber at 11 K. Subsequently, helium was released at 35 K and analysed in a VG5400 or Helix SFT mass spectrometer. A CRONUS-P pyroxene standard analyzed in the same batch as the heating extractions yielded a ^{3}He concentration of 4.76±0.20 x 10^{9} at/g (2σ error), which is consistent within error with the mean ^{3}He concentration of 4.91±0.10 x 10^{9} at/g determined earlier at the GFZ for seven aliquots of this standard and also with the "global mean" from six different labs of 5.02±0.12 x 10^{9} at/g (Blard et al., 2015). Details of the noble gas analytical procedures and the data reduction as well as calibration methods can be found in Niedermann et al. (1997) and Blard et al. (2015).

The ^{3}He/^{4}He values of the trapped (magmatic) component agreed within 2σ error limits in all samples (Table 2) and yielded an error-weighted mean (n = 6) of 10.66±0.29 x 10^{-6} (Table 2). In volcanic rocks with negligible amounts of radiogenic ^{4}He and nucleogenic ^{3}He, the amount of cosmogenic helium can be determined using the following equation (Niedermann, 2002):

$$^{3}He_{cosm} = [(^{3}He/^{4}He)_{meas} - (^{3}He/^{4}He)_{tr}] \times {}^{4}He_{meas} \qquad (2)$$

where the subscripts cosm, meas, and tr denote the cosmogenic, the measured, and the trapped component. Radiogenic He (i.e. $^{4}He_{rad}$) is formed by radioactive decay of U and Th, whereas nucleogenic ^{3}He is mainly generated by thermal-neutron capture reactions involving Li (e.g. Niedermann, 2002). To evaluate whether significant amounts of radiogenic or nucleogenic helium are present in our samples, we analyzed all basalt samples and aliquots of four olivine separates for U, Th, and Li using ICP-MS. Uranium and thorium contents of the basalts range from 2.0 to 2.6 ppm and 8.8 to 10.2 ppm, respectively. The U and Th concentrations in olivine are 0.004–0.02 ppm and 0.01–0.06 ppm, respectively. To correct for $^{4}He_{rad}$ present in our samples we used the approach of Blard and Farley (2008) and determined a correction factor R, which depends on the U and Th concentrations in the phenocrysts and the basalt matrix, the phenocryst size, and the cosmogenic ^{3}He production rate. As the latter is elevation-dependent, we split the samples into two elevation groups and used the highest and lowest U and Th concentrations of the olivine and whole rock samples, respectively, to calculate R-values for a mean phenocryst diameter of 750 µm. Using the equations given in Blard and Farley (2008), we obtained an R-value of 0.94±0.01 for samples from an elevation below 200 m (13T2, 13T3, 13T14) and an R-value of 0.96±0.01 for the remaining samples. Application of these R-factors increased the $^{3}He_{cosm}$ concentrations by 6% and 4%, respectively. Both the uncorrected $^{3}He_{cosm}$

concentrations calculated with equation 2 above, as well as the $^{3}He_{cosm}$ concentrations corrected for $^{4}He_{rad}$ are reported in Table 2.

The production of nucleogenic ^{3}He and of cosmogenic ^{3}He from thermalized cosmic ray neutrons in minerals such as olivine or pyroxene is only significant if the Li content of these minerals exceeds ~5 ppm (Dunai et al., 2007). As the Li concentrations of the analyzed olivine separates are between 1.6 and 2.2 ppm, the production rates of nucleogenic ^{3}He and thermal neutron-produced cosmogenic ^{3}He are so low (<1 at g^{-1} yr^{-1}; Dunai et al., 2007) that corrections are unnecessary.

After the completion of the experimental part of this study, Protin et al. (2016) have reported a hitherto unknown effect of irreversible atmospheric He adsorption on crushed olivine grains, which may lead to an underestimate of cosmogenic ^{3}He if the samples used for pyrolysis contained grains smaller than ~125 µm and the adsorbed component was unaccounted for. As we retrieved the sample material from the crusher without removing small grains, such an effect might potentially affect our results. However, though a rigorous assessment is difficult in hindsight, we argue that a significant influence is unlikely in our case: (1) The crushing efficiency of our manual crusher is not very high, and based on optical inspection of the samples during preparation for pyrolysis the fraction of very small grains is rather small. (2) While the samples of Protin et al. (2016) were heated to less than 100°C for only 12 hours before pyrolysis, in our case the sample carrousel was baked at 100°C for one week. This procedure may have helped to reduce any atmospheric He contamination, even though Protin et al. (2016) observed that for their samples heating to 500-900°C for 15 minutes was still insufficient to release the atmospheric component completely. (3) In another project performed in the GFZ noble gas lab (Baynes et al., 2015), one out of three very He-poor olivine samples (3-4 x 10^{-10} cm^{3} STP/g) from a single lava flow was used for pyrolysis without prior crushing; however the He concentration (both considering pyrolysis only or the sum of pyrolysis and crusher extraction) in the samples DW5 and DW7 crushed beforehand did not exceed that in the uncrushed sample DW6 beyond error limits. We are therefore confident that the effect described by Protin et al. (2016) does not significantly affect our results.

5. Calculation of surface exposure ages

Both the ^{3}He and ^{10}Be exposure ages (Tables 2, 3) were computed with the CRONUScalc online calculator (http://web1.ittc.ku.edu:8888/2.0; version 2.0; Marrero et al., 2016), which employs cosmogenic nuclide production rates determined at several primary calibration sites (Borchers et al., 2016). For the nuclides ^{3}He and ^{10}Be, those production rates are based on the studies by

Goehring et al. (2010), Putnam et al. (2010), Kelly et al. (2015), and Lifton et al. (2015). We used the time-dependent production rate scaling model of Lal (1991) – Stone (2000) (= Lm model) to calculate the exposure ages shown in Table 2 and Table 3. In addition, we report exposure ages computed with the scaling model of Lifton et al. (2014) (= LSD model) (Tables A.1, A.2). As other available scaling models, which are based on neutron monitor data (Dunai, 2001; Lifton et al., 2005; Desilets et al., 2006), result in a poorer fit of the primary calibration data sets (Borchers et al., 2016), we do not report exposure ages for these scaling frameworks. We note, however, that the respective ages would fall between the ages derived with the Lm and LSD models.

The internal errors of the exposure ages (Tables 2, 3) are based on analytical uncertainties only, while the total errors given by CRONUScalc also include the uncertainties of the local ^{3}He and ^{10}Be production rates (see Marrero et al., 2016 for details). The internal and total errors are reported as 1σ. All ages were calculated assuming no erosion. For two samples (13T9 and 13T12), we also report ^{3}He ages that were obtained by assuming a total erosion of 2 cm and 10 cm, respectively, based on our field observations (section 3). For the two aliquots analyzed of sample 13T4, we also report an error-weighted mean age.

6. Discussion

6.1 The Holocene eruption history of the Kula volcanic field

In this section we discuss the ^{3}He exposure ages obtained for samples from lava flows and cinder cones (Table 2) and the ^{10}Be ages for the quartz-bearing xenoliths (Table 3) from the Kula volcanic field. Two of the four exposure ages for the westernmost block lava flow agree very well: the ^{3}He age of 2.5±0.4 ka for sample 13T14 collected near Demirköprü dam and the mean ^{10}Be age of 2.4±0.3 ka for the augen gneiss xenolith (13T4) north of Adala (Fig. 4). We consider the ^{3}He age as particularly robust, because sample 13T14 was taken from a smooth and pristine flow surface (Fig. 3b). The ^{3}He age is supported by the almost identical ^{10}Be age of the gneiss xenolith, which is another indication that atmospheric He contamination introduced by crushing (Protin et al., 2016), which would cause an underestimate of the ^{3}He age, is not a problem for our samples. Also, a significant inherited ^{10}Be component in the xenolith due to near-surface exposure prior to its incorporation in the lava flow is unlikely, as this would lead to an overestimate of the ^{10}Be age, thus further impairing the agreement between the two methods. The two other ^{3}He ages for the same flow, which were derived from samples of basalt blocks, are considered less reliable (Fig. 4). The age of 1.5±0.3 ka for the larger block (with a diameter of ~1.5 m) is still consistent with the older nominal ages, when considering their 2σ errors. However, the ^{3}He age of 0.7±0.4 ka for the smaller block (~0.8 m in diameter) is not. We interpret the latter to underestimate the emplacement of the block lava flow, probably owing to a later tilting of this relatively small block.

In the central part of the Kula volcanic field, the basalt sample from the flank of the cinder cone west of Sandal village (13T6; Fig. 3e) yielded a ^{3}He age of 2.6±0.4 ka. An identical ^{10}Be age of 2.6±0.3 ka was obtained for the quartz-bearing xenolith (13T5) from the same cinder cone (Fig. 4), again demonstrating the reliability of our results. The position of the xenolith sample at the top of the cone, its round shape (Fig. 3d), and its lithology – which differs from the rocks exposed in the surroundings of the cone (mainly augen gneisses) – indicate that the sample originates from the metamorphic basement underneath the cone and was trapped by the rising magma during the course of the last eruption. Hence, an inherited ^{10}Be component can be excluded. We interpret the two ages of ~2.6 ka to date the last eruption of the small cinder cone near Sandal. For the large lava flow located northwest of the cone, sample 13T7 (Fig. 3c) provides a somewhat older ^{3}He exposure age (i.e. 3.3±0.4 ka). Field relations demonstrate that this flow originated from the *Karadivlit Tepe* cinder cone, which is located in the southeastern part of the flow (Fig. 2).

In the eastern part of the volcanic field, sample 13T9 from a β4 basalt flow yielded a ^{3}He exposure age of 0.9±0.2 ka (Fig. 4). The sample was taken from a rather smooth flow surface surrounded by block lava and therefore we consider the ^{3}He age as reliable, even though the sampled surface may have been slightly eroded. Considering an erosion of 2 cm, as estimated in the field (see section 3), increases the exposure age by only 10 years (Table 2). Two previous studies (Westaway et al., 2006; van Gorp et al., 2013) that attempted to date the same β4 flow with K-Ar and luminescence methods inferred older ages, which will be discussed in more detail in the following section.

The quartz-bearing metasedimentary xenolith (13T15) from the top of *Çakallar Tepe* yielded a ^{10}Be exposure age of 11.2±1.1 ka (Fig. 4). An inherited ^{10}Be component can again be ruled out, because the fine-grained xenolith is different from the coarse-grained augen gneisses exposed around *Çakallar Tepe*. Hence, the xenolith originates from a different lithotectonic unit and must have been entrained in the rising basalt magma at considerable depth beneath the cone. The relatively high ^{10}Be age – as compared to the ages for the younger lava flows discussed above – is consistent with the presence of thin patches of soil on subhorizontal parts of the crater rim. Of course, despite the fresh appearance of the sampled surface we cannot exclude a minor influence of erosion, which would make the ^{10}Be age slightly too low. Nevertheless, we interpret the ^{10}Be age of the xenolith to closely date the last eruption of the

Çakallar Tepe cinder cone. If this is correct, it provides an important age constraint for the famous fossil human footprints that occur in the ash deposits of this cone (Fig. 3f). Our ^{10}Be age is considerably younger than the two thermoluminescence (TL) ages of 49±9 ka and 26±5 ka obtained for the footprints and the overlying scoria deposits (Göksu, 1978). Apart from the fact that the scoria deposits, which protected the footprints from erosion, belong to the same eruption cycle as the ash layer (Barnaby, 1975), the different TL ages are incompatible with the assumption of Göksu (1978) that the scoria has reset the TL clock of the ash layer. If this were the case, both TL ages should be identical within errors. For this reason, we argue that both thermoluminescence ages are too old and overestimate the last eruption of *Çakallar Tepe*.

The sample from the β3 lava flow east of Yeniköy village (13T12) yielded a ^{3}He exposure age of 13.1±1.6 ka (Fig. 4). Field observations indicate that the sampling site on this flow experienced 10±5 cm of erosion (see section 3). Taking into account ten centimeters of erosion at a steady rate increases the exposure age to 14.2±1.8 ka (Table 2).

6.2 Comparison of exposure ages with previously published K-Ar and luminescence ages

Compared to previously published K-Ar ages for β3 lava flows in the northern part of the volcanic field, which range from ~240 ka to ~80 ka (Westaway et al., 2004, 2006), our ^{3}He exposure age of ~13 ka for the β3 flow east of Yeniköy is much younger. Neither erosion nor shielding are sufficient to explain the marked difference between the K-Ar ages and the ^{3}He age. Our field observations indicate that the surface of the lava flow near Yeniköy is better preserved and therefore indeed younger than the β3 lava flows which were hitherto targeted for K-Ar dating. We therefore suggest that the lava flows and cinder cones previously assigned to the β3 group (e.g. Richardson-Bunbury, 1996) encompass a wider time span than previously envisaged. Our ^{10}Be exposure age of 11.2±1.1 ka for *Çakallar Tepe* indicates that the last eruption of this cone occurred during the β3 phase as well, and not during the phase β4 as suggested by Ercan (1981 unpublished dissertation, Istanbul Technical University, cited in Richardson-Bunbury, 1996). Our new exposure ages suggest that if the eruption phases β3 and β4 are indeed separated in time, the period of volcanic quiescence started at about 11 ka and ended with the emplacement of the lava flow near Sandal at 3.3±0.4 ka (Fig. 4).

Our ^{3}He exposure age of 0.9±0.2 ka for the large lava flow north of Kula is considerably younger than two K-Ar ages of 7±2 and 4±2 ka derived for samples taken near the northern end of the same flow (Westaway et al., 2006) (Fig. 4). The age difference could be explained by the presence of minor amounts of excess Ar, which would cause the K-Ar age to overestimate the emplacement of the flow (e.g. Laughlin et al., 1994). This inference is supported by three luminescence ages which bracket the emplacement of the same lava flow that led to the damming of the Gediz River (van Gorp et al., 2013). A sand sample from fluvial sediments underneath the flow yielded a multiple-grain feldspar age of 3.0±0.2 ka, whereas single-grain feldspar ages of 2.6±0.4 and 2.1±0.5 ka (1σ errors) were obtained for sediments resting on top of the flow (van Gorp et al., 2013). Although the luminescence ages indicate that the eruption of the flow is younger than the nominal K-Ar ages, they are still somewhat older than our ^{3}He exposure age. One reason for this discrepancy may be that the luminescence ages overestimate the deposition of the respective fluvial sediments due to incomplete signal resetting, even though the minimum age model (cf. Galbraith et al., 1999) was applied.

7. Conclusions

To the best of our knowledge, this study is the first to combine ^{3}He exposure dating of olivine from mafic volcanic rocks with ^{10}Be exposure dating of quartz-bearing xenoliths to quantify eruption ages of cinder cones and basaltic lava flows in a Late Quaternary volcanic field. The two exposure dating methods yielded consistent results for Holocene volcanic rocks in the Kula volcanic field (Western Turkey) and indicate a period of pronounced volcanic activity that began less than 4000 years ago. Moreover, a ^{10}Be age of 11.2±1.1 ka (1σ) provides an important age constraint for the famous human footprints that are preserved in volcanic ash deposits of the volcanic field. More generally, our results demonstrate that cosmogenic nuclides can be applied to date very young volcanic rocks, even in regions of low elevation where nuclide production rates are low. Hence, exposure dating provides a powerful alternative to K-Ar or ^{40}Ar/^{39}Ar dating of young volcanic rocks.

Acknowledgements

We thank Nicole Stroncik, Enzio Schnabel, and Heike Rothe (GFZ Potsdam) for their help in the chemical treatment of the olivine separates, the helium analysis of olivine, and the ICP-MS analysis of whole rock and olivine samples, respectively. Anne Niehus (University of Münster) is thanked for her help during ^{10}Be separation from quartz and target preparation. Marcus Christl (ETH Zurich) is kindly acknowledged for the AMS analysis of the ^{10}Be targets. Finally, we are indebted to the Kula Municipality for providing the photograph of the human footprints depicted in Figure 3. A thorough review by P.-H. Blard improved and clarified many aspects of this manuscript.

References

Akdeniz, E., 2011. Some evidence on the first known residents of Katakekaumene (Burned Lands). Mediterranean Archaeology and Archaeometry 11, 69–74.

Alıcı, P., Temel, A., Gourgaud, A., 2002. Pb–Nd–Sr isotope and trace element geochemistry of Quaternary extension-related alkaline volcanism: a case study of Kula region (western Anatolia, Turkey). Journal of Volcanology and Geothermal Research 115, 487–510.

Ammon, K., Dunai, T.J., Stuart, F.M., Meriaux, A.-S., Gayer, E., 2009. Cosmogenic ^{3}He exposure ages and geochemistry of basalts from Ascension Island, Atlantic Ocean. Quaternary Geochronology 4, 525–532.

Balco, G., Stone, J.O., 2003. Measuring the density of rock, sand, till, etc. UW Cosmogenic Nuclide Laboratory, methods and procedures. http://depts.washington.edu/cosmolab/chem.html (visited 21.05.2015).

Barnaby, W., 1975. News and views. Nature 254, 553.

Baynes, E.R.C., Attal, M., Niedermann, S., Kirstein, L.A., Dugmore, A.J., Naylor, M., 2015. Erosion during extreme flood events dominates Holocene canyon evolution in northeast Iceland. Proceedings of the National Academy of Sciences of the United States of America 112, 2355–2360.

Blard, P.-H., Farley, K.A., 2008. The influence of radiogenic ^{4}He on cosmogenic ^{3}He determinations in volcanic olivine and pyroxene. Earth and Planetary Science Letters 276, 20–29.

Blard, P.-H., Balco, G., Burnard, P.G., Farley, K.A., Fenton, C.R., Friedrich, R., Jull, A.J.T., Niedermann, S., Pik, R., Schaefer, J.M., Scott, E.M., Shuster, D.L., Stuart, F.M., Stute, M., Tibari, B., Winckler, G., Zimmermann, L., 2015. An inter-laboratory comparison of cosmogenic ^{3}He and radiogenic ^{4}He in the CRONUS-P pyroxene standard. Quaternary Geochronology 26, 11–19.

Borchers, B., Marrero, S., Balco, G., Caffee, M., Goehring, B., Lifton, N., Nishiizumi, K., Phillips, F., Schaefer, J., Stone, J., 2016. Geological calibration of spallation production rates in the CRONUS-Earth project. Quaternary Geochronology 31, 188–198.

Borsi, S., Ferrara, G. Innocenti, F., Mazzuoli, R., 1972. Geochronology and petrology of recent volcanics in the Eastern Aegean Sea (West Anatolia and Lesvos Island). Bulletin Volcanologique 36, 473–496.

Bozkurt, E., 2000. Timing of extension on the Büyük Menderes Graben, western Turkey, and its tectonic implications. In: Bozkurt, E., Winchester, J.A., Piper, J.D.A. (Eds.), Tectonics and Magmatism in Turkey and the Surrounding Area. Geological Society of London Special

Publications 173, 385–403.

Brun, J.-P., Sokoutis, D., 2010. 45 m.y. of Aegean crust and mantle flow driven by trench retreat. Geology 38, 815–818.

Buscher, J.T., Hampel, A., Hetzel, R., Dunkl, I., Glotzbach, C., Struffert, A., Akal, C., Rätz, M., 2013. Quantifying rates of detachment faulting and erosion in the central Menderes Massif (western Turkey) by thermochronology and cosmogenic ^{10}Be. Journal of the Geological Society of London 170, 669–683.

Canet, J., Jaoul, P., 1946. Report on the geology of the Manisa-Aydın-Kula-Gördes area. Unpublished report no. 2068. General Directorate of Mineral Research and Exploration, Ankara (in Turkish).

Chmeleff, J., von Blanckenburg, F., Kossert, K., Jakob, D., 2010. Determination of the ^{10}Be half-life by multicollector ICP-MS and liquid scintillation counting. Nuclear Instruments and Methods in Physics Research B 268, 192–199.

Christl, M., Vockenhuber, C., Kubik, P.W., Wacker, L., Lachner, J., Alfimov, V., Synal, H.-A., 2013. The ETH Zurich AMS facilities: Performance parameters and reference materials. Nuclear Instruments and Methods in Physics Research B 294, 29–38.

Craig, H., Poreda, R.J., 1986. Cosmogenic ^{3}He in terrestrial rocks: The summit lavas of Maui. Proceedings of the National Academy of Sciences USA 83, 1970–1974.

Desilets, D., Zreda, M.G., Prabu, T., 2006. Extended scaling factors for in situ cosmogenic nuclides: New measurements at low latitude. Earth and Planetary Science Letters 246, 265–276.

Dunai, T.J., 2001. Influence of secular variation of the geomagnetic field on production rates of in situ produced cosmogenic nuclides. Earth and Planetary Science Letters 193, 197–212.

Dunai, T.J., Stuart, F.M., Pik, R., Burnard, P., Gayer, E., 2007. Production of ^{3}He in crustal rocks by cosmogenic thermal neutrons. Earth and Planetary Science Letters 258, 228–236.

Ercan, T., Satır, M., Kreuzer, H., Türkecan, A., Günay, E., Çevikbaş, A., Ateş, M., Can, B., 1985. Interpretation of new chemical, isotopic and radiometric data on Cenozoic volcanics of western Anatolia. Türkiye Jeoloji Kurumu Bülteni (Bulletin of the Geological Society of Turkey) 28, 121–136 (in Turkish with English abstract).

Faccenna, C., Jolivet, L., Piromallo, C., Morelli, A., 2003. Subduction and the depth of convection in the Mediterranean mantle. Journal of Geophysical Research 108, 2099, doi:10.1029/2001JB001690.

Foeken, J.P.T., Stuart, F.M., Francalanci, L., 2009. Dating Holocene lavas on Stromboli, Italy using cosmogenic He. Quaternary Geochronology 4, 517–524.

Fytikas, M., Innocenti, F., Manetti, P., Mazzuoli, R., Peccerillo, A., Villari, L., 1984. Tertiary to Quaternary evolution of volcanism in the Aegean region. In: Dixon, J.E., Robertson, A.H.F. (Eds.), The Geological Evolution of the Eastern Mediterranean. Geological Society of London Special Publications 17, 687–699.

Galbraith, R.F., Roberts, R.G., Laslett, G.M., Yoshida, H., Olley, J.M., 1999. Optical dating of single and multiple grains of quartz from Jinmium rock shelter, northern Australia: Part I. Experimental design and statistical models. Archaeometry 41, 339–364.

Glodny, J., Hetzel, R., 2007. Precise U-Pb ages of syn-extensional Miocene intrusions in the central Menderes Massif, western Turkey. Geological Magazine 144, 235–246.

Goehring, B.M., Kurz, M.D., Balco, G., Schaefer, J.M., Licciardi, J., Lifton, N., 2010. A reevaluation of in situ cosmogenic ^{3}He production rates. Quaternary Geochronology 5, 410–418.

Goethals, M.M., Hetzel, R., Niedermann, S., Wittmann, H., Fenton, C.R., Kubik, P.W., Christl, M., von Blanckenburg, F., 2009. An improved experimental determination of cosmogenic ^{10}Be/^{21}Ne and ^{26}Al/^{21}Ne production ratios in quartz. Earth and Planetary Science Letters 284, 187–198.

Göksu, H.Y., 1978. The TL age determination of fossil human footprints. Archaeo-Physika 10, 455–462.

Güleç, N., 1991. Crust-mantle interaction in western Turkey: implications from Sr and Nd isotope geochemistry of Tertiary and Quaternary volcanics. Geological Magazine 128, 417–435.

Hamilton, W.J., Strickland, H.E., 1841. On the geology of the western part of Asia Minor. Transactions of the Geological Society London 6, 1–39.

Innocenti, F., Agostini, S., di Vincenzo, G., Doglioni, C., Manetti, P., Savaşçin, M.Y., Tonarini, S., 2005. Neogene and Quaternary volcanism in Western Anatolia: Magma sources and geodynamic evolution. Marine Geology 221, 397–421.

Kayan, I., 1992. Demirköprü baraj gölü batı kıyısında Çakallar volkanizması ve fosil insan ayak izleri. Ege Coğrafya Dergisi, Cilt 6, 1–34 (in Turkish with English summary).

Kelly, M.A., Lowell, T.V., Applegate, P.J., Phillips, F.M., Schaefer, J.M., Smith, C.A., Kim, H., Leonard, K.C., Hudson, A.M., 2015. A locally calibrated, late glacial ^{10}Be production rate from a low-latitude, high-altitude site in the Peruvian Andes. Quaternary Geochronology 26, 70–85.

Kohl, C.P., Nishiizumi, K., 1992. Chemical isolation of quartz for measurement of in-situ-produced cosmogenic nuclides. Geochimica et Cosmochimica Acta 56, 3583–3587.

Korschinek, G., Bergmaier, A., Faestermann, T., Gerstmann, U.C., Knie, K., Rugel, G., Wallner, A., Dillmann, I., Dollinger, G., Lierse von Gostomski, Ch., Kossert, K., Maiti, M., Poutivtsev, M., Remmert, A., 2010. A new value for the half-life of ^{10}Be by Heavy-Ion Elastic Recoil Detection and liquid scintillation counting. Nuclear Instruments and Methods in Physics Research B 268, 187–191.

Kubik, P.W., Christl, M., 2010. ^{10}Be and ^{26}Al measurements at the Zurich 6 MV Tandem AMS facility. Nuclear Instruments and Methods in Physics Research B 268, 880–883.

Lal, D., 1991. Cosmic ray labeling of erosion surfaces: in situ nuclide production rates and erosion models. Earth and Planetary Science Letters 104, 424–439.

Laughlin, A.W., Poths, J., Healey, H.A., Reneau, S., WoldeGabriel, G., 1994. Dating of Quaternary basalts using the cosmogenic ^{3}He and ^{14}C methods with implications for excess ^{40}Ar. Geology 22, 135–138.

Lifton, N.A., Bieber J.W., Clem, J.M., Duldig, M.L., Evenson, P., Humble, J.E., Pyle, R., 2005. Addressing solar modulation and long-term uncertainties in scaling secondary cosmic rays for in situ cosmogenic nuclide applications. Earth and Planetary Science Letters 239, 140–161.

Lifton, N., Sato, T., Dunai, T.J., 2014. Scaling in situ cosmogenic nuclide production rates using analytical approximations to atmospheric cosmic-ray fluxes. Earth and Planetary Science Letters 386, 149–160.

Lifton, N., Caffee, M., Finkel, R., Marrero, S., Nishiizumi, K., Phillips, F.M., Goehring, B., Gosse, J., Stone, J., Schaefer, J., Theriault, B., Jull, A.J.T., Fifield, K., 2015. In situ cosmogenic nuclide production rate calibration for the CRONUS-Earth project from Lake Bonneville, Utah, shoreline features. Quaternary Geochronology 26, 56–69.

Maddy, D., Demir, T., Veldkamp, A., Bridgland, D.R., Stemerdink, C., van der Schriek, T., Schreve, D., 2012. The obliquity-controlled early Pleistocene terrace sequence of the Gediz River, western Turkey: a revised correlation and chronology. Journal of the Geological Society London 169, 67–82.

Marchetti, D.M., Hynek, S.A., Cerling, T.E., 2014. Cosmogenic ^{3}He exposure ages of young lava flows in the northwestern Payún Matru volcanic field, Mendoza Province, Argentina. Quaternary Geochronology 19, 67–75.

Marrero, S.M., Phillips, F.M., Borchers, B., Lifton, N., Aumer, R., 2016. Cosmogenic nuclide systematics and the CRONUScalc program. Quaternary Geochronology 31, 160–187.

Niedermann, S., 2002. Cosmic-ray produced noble gases in terrestrial rocks: dating tools for surface processes. In: Porcelli, D., Ballentine, C.J., Wieler, R. (Eds.), Noble Gases in

Geochemistry and Cosmochemistry. Reviews in Mineralogy and Geochemistry 47, 731–784.
Niedermann, S., Bach, W., Erzinger, J., 1997. Noble gas evidence for a lower mantle component in MORBs from the southern East Pacific Rise: Decoupling of helium and neon isotope systematics. Geochimica et Cosmochimica Acta 61, 2697–2715.
Nishiizumi, K., Imamura, M., Caffee, M.W., Southon, J.R., Finkel, R.C., McAninch, J., 2007. Absolute calibration of ^{10}Be AMS standards. Nuclear Instruments and Methods in Physics Research B 258, 403–413.
Nomade, S., Genty, D., Sasco, R., Scao, V., Féruglio, V., Baffier, D., Guillou, H., Bourdier, C., Valladas, H., Reigner, E., Debard, E., Pastre, J.-F., Geneste, J.-M., 2016. A 36,000-year-old volcanic eruption depicted in the Chauvet-Pont d'Arc Cave (Ardèche, France)? PLoS ONE 11, e0146621, doi:10.1371/journal.pone.0146621.
Ozansoy, F., 1969. Türkiye pleistosen fosil insan ayak izleri. Maden Tetkik ve Arama Enstitüsü Dergisi 72, 204–209.
Paton, S.M., 1992. The relationship between expansion and volcanism in western Turkey, the Aegean Sea, and central Greece. PhD thesis. Cambridge University.
Phillips, F.M., Argento, D.C., Balco, G., Caffee, M.W., Clem, J., Dunai, T., Finkel, R., Goehring, B., Gosse, J.C., Hudson, A., Jull, T.A., Kelly, M., Kurz, M., Lal, D., Lifton, N., Marrero, S.M., Nishiizumi, K., Reedy, R., Schaefer, J., Stone, J.O., Swanson, T., Zreda, M.G., 2016. The CRONUS-earth project: a synthesis. Quaternary Geochronology 31, 119–154.
Prelević, D., Akal, C. Foley, S.F., Romer, R.L., Stracke, A., van den Bogaard, P., 2012. Ultrapotassic mafic rocks as geochemical proxies for post-collisional dynamics of orogenic lithospheric mantle: the case of southwestern Anatolia, Turkey. Journal of Petrology 53, 1019–1055.
Protin M., Blard P.-H., Marrocchi Y., Mathon F., 2016. Irreversible adsorption of atmospheric helium on olivine: A lobster pot analogy. Geochimica et Cosmochimica Acta 179, 76–88.
Purvis, M., Robertson, A., 2004. A pulsed extension model for the Neogene-Recent E-W-trending Alaşehir Graben and the NE-SW-trending Selendi and Gordes Basins, western Turkey. Tectonophysics 391, 171–201.
Putnam, A., Schaefer, J.M., Barrell, D.J.A., Vandergoes, M., Denton, G.H., Kaplan, M.R., Finkel, R.C., Schwartz, R., Goehring, B.M., Kelley, S.E., 2010. In situ cosmogenic ^{10}Be production-rate calibration from the Southern Alps, New Zealand. Quaternary Geochronology 5, 392–409.

Radt, S., 2004. Strabons Geographika. Translated and commented by S. Radt (editor), vol. 3, p. 653, 1st edition, 680 pages, Vandenhoeck & Ruprecht, Göttingen.

Richardson-Bunbury, J.M., 1996. The Kula Volcanic Field, western Turkey: the development of a Holocene alkali basalt province and the adjacent normal-faulting graben. Geological Magazine 133, 275–283.

Schmitt, A.K., Danišík, M., Aydar, E., Şen, E., Ulusoy, İ., Lovera, O.M., 2014. Identifying the volcanic eruption depicted in a Neolithic painting at Catalhöyük, Central Anatolia, Turkey. PLoS ONE 9, e84711, doi:10.1371/journal.pone.0084711.

Şen, E., Aydar, E., Bayhan, H., Gourgaud, A., 2014. Alkali Bazalt ve Piroklastik Çökellerin Volkanolojik Özellikleri, Kula Volkanları, Batı Anadolu. Volcanological Characteristics of Alkaline Basalt and Pyroclastic Deposits, Kula Volcanoes, Western Anatolia. Bulletin of the Earth Sciences Application and Research Centre of Hacettepe University 35, 219–252 (in Turkish with English abstract).

Seyitoğlu, G., Scott, B.C., 1991. Late Cenozoic extension and basin formation in west Turkey. Geological Magazine 128, 155–166.

Stone, J.O., 2000. Air pressure and cosmogenic isotope production. Journal of Geophysical Research 105, 23753–23759.

Tekkaya, İ., 1976. İnsanlara ait fosil ayak izleri. Yeryuvarı ve İnsan Dergisi (July 1976), 8–10 (in Turkish with English abstract).

Thomson, S.N., Ring, U., 2006. Thermochronologic evaluation of postcollision extension in the Anatolide orogen, western Turkey. Tectonics 25, TC3005, doi:10.1029/2005TC001833.

van Gorp, W., Veldkamp, A., Temme, A.J.A.M., Maddy, D., Demir, T., van der Schriek, T., Reimann, T., Wallinga, J., Wijbrans, J., Schoorl, J.M., 2013. Fluvial response to Holocene volcanic damming and breaching in the Gediz and Geren rivers, Western Turkey. Geomorphology 201, 430–448.

Westaway, R., Pringle, M., Yurtmen, S., Demir, T., Bridgland, D., Rowbotham, G., Maddy, D., 2004. Pliocene and Quaternary regional uplift in western Turkey: the Gediz River terrace staircase and the volcanism at Kula. Tectonophysics 391, 121–169.

Westaway, R., Guillou, H., Yurtmen, S., Beck, A., Bridgland, D., Demir, T., Scaillet, S., Rowbotham, G., 2006. Late Cenozoic uplift of western Turkey: Improved dating of the Kula Quaternary volcanic field and numerical modelling of the Gediz River terrace staircase. Global and Planetary Change 51, 131–171.

Table 1
Information on sampling locations and samples collected from lava flows and cinder cones of the Kula volcanic field, western Turkey.

Sample	Latitude [°N]	Longitude [°E]	Elevation [m]	Sample thickness [cm]	Topographic shielding factor[a] –	Total shielding factor[b] –
Basalt samples from β4 flows and cinder cones						
13T2	38.5875	28.2778	129	6	0.9995	0.9562
13T3	38.5876	28.2709	133	6	0.9995	0.9562
13T6	38.5727	28.5613	807	5	0.9989	0.9629
13T7	38.5871	28.5418	719	5	0.9987	0.9627
13T9	38.5826	28.6538	668	5	0.9979	0.9619
13T14	38.6098	28.3010	193	5	0.9915	0.9556
Basalt sample from β3 flow						
13T12	38.5877	28.7705	426	4	0.9999	0.9708
Quartz-bearing xenoliths from two β4 flows and a β3 cinder cone						
13T4	38.5876	28.2712	136	9	0.9809	0.9233
13T5	38.5734	28.5617	842	12	0.9923	0.9026
13T15	38.6506	28.3387	380	6	0.9923	0.9493

[a] The correction factor was determined using the topographic shielding calculator of the CRONUS Earth web calculators (http://web1.ittc.ku.edu:8888/2.0; version 2.0; Marrero et al., 2016). It includes the shielding due to the dip of the sampled surface and the shielding by the surrounding topography.

[b] The total shielding factor includes corrections for sample thickness and topographic shielding. The mean density determined for the basalt samples is 2.3 g cm^{-3}, whereas the density of the quartz-bearing xenoliths was measured as 2.1 g cm^{-3} (13T4), 2.5 g cm^{-3} (13T5), and 2.3 g cm^{-3} (13T15), respectively. See text for further information.

Table 2
Results of He measurements for olivine from basalts of the Kula volcanic field and resulting ^{3}He exposure ages. Error limits are 1σ.

Sample	Weight [g]	Extraction method	^{4}He concentration [10^{-8} cm^3 g^{-1}]	^{3}He/^{4}He [10^{-6}]	$^3He_{cosm}$ [a] and $\mathbf{^3He_{cosm}}$ corrected for $^4He_{rad}$ [b] [10^5 at g^{-1}]	Local production rate [c] [at g^{-1} a^{-1}]	^{3}He exposure age [d] [a]
13T2	0.89196	crushing	0.636 ± 0.013	10.55 ± 0.27	0.70 ± 0.38 | **0.75 ± 0.40**	111.4	670 ± 390 (390)
	0.83450	pyrolysis	0.2292 ± 0.0047	11.79 ± 0.59			
13T3	0.78644	crushing	0.571 ± 0.011	10.10 ± 0.35	1.62 ± 0.26 | **1.73 ± 0.28**	111.8	1530 ± 240 (290)
	0.74248	pyrolysis	0.1706 ± 0.0036	14.16 ± 0.56			
13T6	0.75124	crushing	1.491 ± 0.037	11.01 ± 0.50	4.91 ± 0.68 | **5.12 ± 0.71**	194.8	2610 ± 340 (430)
	0.71874	pyrolysis	0.665 ± 0.013	13.41 ± 0.35			
13T7	0.88110	crushing	1.294 ± 0.032	10.59 ± 0.48	5.92 ± 0.40 | **6.16 ± 0.42**	181.9	3340 ± 230 (420)
	0.96218	pyrolysis	0.2150 ± 0.0043	20.85 ± 0.65			
13T9	0.78618	crushing	0.3053 ± 0.0061	*9.65 ± 0.33*[a]	1.46 ± 0.34 | **1.52 ± 0.35**	174.5	880 ± 210 (240) [890 ± 220 (240)]
	0.74050	pyrolysis	0.1453 ± 0.0031	14.43 ± 0.84			
13T12	0.65080	crushing	1.379 ± 0.028	10.98 ± 0.27	18.9 ± 0.9 | **19.7 ± 1.0**	145.1	13100 ± 700 (1600) [14200 ± 800 (1800)]
	0.61502	pyrolysis	1.163 ± 0.023	16.70 ± 0.23			
13T14	0.74982	crushing	0.637 ± 0.016	10.91 ± 0.48	2.80 ± 0.41 | **2.97 ± 0.43**	117.7	2520 ± 350 (440)
	0.71134	pyrolysis	0.3689 ± 0.0074	13.48 ± 0.38			

[a] For quantification of the cosmogenic ^{3}He concentration ($^3He_{cosm}$), a $(^3He/^4He)_{tr}$ value of (10.66 ± 0.14) x 10^{-6} was used, which is the error-weighted mean of all crushing extractions excluding sample 13T9. For the latter sample the ^{3}He/^{4}He ratio measured after crushing is low due to a technical problem (bad alignment of the ^{3}He and ^{4}He peaks in the Helix mass spectrometer) that was only recognized during the subsequent calibration gas measurement. The $^3He_{cosm}$ concentrations were calculated as explained in the text.

[b] The correction for radiogenic ^{4}He follows the approach of Blard and Farley (2008). The uncorrected cosmogenic ^{3}He concentration was divided by a factor R of 0.94 ± 0.01 (for samples 13T2, 13T3, 13T14) or 0.96 ± 0.01 (samples 13T6, 13T7, 13T9, 13T12) (see text for details).

[c] These are local, depth-averaged production rates, which consider sample thickness and topographic shielding.

[d] The ^{3}He exposure ages were calculated with the CRONUScalc online calculator (http://web1.ittc.ku.edu:8888/2.0; version 2.0; Marrero et al., 2016) using the time-dependent scaling model of Lal (1991) – Stone (2000). The internal errors of the exposure ages are based on the analytical uncertainty only. The total uncertainties provided by CRONUScalc also include the uncertainty of the local ^{3}He production rate and are given in parentheses (Marrero et al., 2016; Phillips et al., 2016). ^{3}He exposure ages given in square brackets for samples 13T9 and 13T12 were obtained assuming a steady erosion rate that leads to a total erosion of 2 cm and 10 cm, respectively (as discussed in the text).

Table 3
^{10}Be concentrations, local production rates and ^{10}Be exposure ages. Error limits are 1σ.

Sample	^{10}Be concentration [a]	Production rate (spallation) [b]	Production rate (muons) [b]	^{10}Be exposure age [c]	
	[10^3 at g^{-1}]	[at g^{-1} a^{-1}]	[at g^{-1} a^{-1}]	[a]	
13T4a	7.0 ± 1.3	3.70	0.058	1840 ± 340 (370)	Mean age 2350 ± 230 (270)
13T4b	10.8 ± 1.3	3.70	0.058	2860 ± 320 (390)	
13T5	16.7 ± 1.6	6.41	0.080	2600 ± 240 (300)	
13T15	54.8 ± 3.2	4.68	0.065	11200 ± 700 (1100)	

[a] Blank-corrected ^{10}Be concentrations. Propagated analytical errors include the error based on counting statistics and the error of the blank correction. ^{10}Be concentrations were measured at ETH Zurich and are normalized to the secondary standard S2007N with a nominal $^{10}Be/^{9}Be$ ratio of 28.1×10^{-12} (Kubik and Christl, 2010), considering the ^{10}Be half-life of 1.387 ± 0.012 Ma (Chmeleff et al., 2010; Korschinek et al., 2010). The secondary standard has been calibrated to the primary standard ICN 01-5-1 (Nishiizumi et al., 2007; Kubik and Christl, 2010). Note that the secondary standard S2007N is identical to the 07KNSTD standardization.

[b] These are local, depth-averaged production rates, which consider sample thickness and topographic shielding.

[c] The ^{10}Be exposure ages were calculated with the CRONUScalc online calculator (http://web1.ittc.ku.edu:8888/2.0; version 2.0; Marrero et al., 2016) using the time-dependent scaling model of Lal (1991) – Stone (2000). The internal errors of the exposure ages are based on the analytical uncertainty only. The total uncertainties provided by CRONUScalc also include the uncertainty of the local ^{10}Be production rate and are given in parentheses (Marrero et al., 2016; Phillips et al., 2016). The 2.7% error of the secondary AMS standard S2007N relative to the primary standard ICN-01-5-1 (Kubik and Christl, 2010) is not included in these uncertainties.

Table A.1
^{3}He exposure ages[a] for two different scaling-models. Error limits are 1σ.

Sample	Lal (1991) – Stone (2000) time-dependent Lm[b] [a]	Lifton et al. (2014) LSD[c] [a]
13T2	670 ± 390 (390)	740 ± 430 (450)
13T3	1530 ± 240 (290)	1800 ± 370 (500)
13T6	2610 ± 340 (430)	3000 ± 430 (610)
13T7	3340 ± 230 (420)	3850 ± 260 (640)
13T9	880 ± 210 (240)	960 ± 250 (290)
13T12	13100 ± 700 (1600)	15000 ± 670 (2300)
13T14	2520 ± 350 (440)	2970 ± 470 (650)

[a] The ^{3}He exposure ages were calculated with the CRONUScalc online calculator (http://web1.ittc.ku.edu:8888/2.0; version 2.0; Marrero et al., 2016) using two different scaling models. The internal errors of the exposure ages are based on the analytical uncertainty only. The total uncertainties provided by CRONUScalc also include the uncertainty of the local ^{3}He production rate and are given in parentheses (Marrero et al., 2016; Phillips et al., 2016).

[b] The Lal (1991) – Stone (2000) time-dependent scaling model is referred to as the "Lm model" in section 5 and the CRONUScalc online calculator.

[c] The time-dependent scaling model of Lifton et al. (2014) is referred to as "LSD model" in section 5. The LSD scaling model has the abbreviation "Sf" in CRONUScalc (Marrero et al., 2016).

Table A.2
^{10}Be exposure ages[a] for two different scaling-models. Error limits are 1σ.

Sample	Lal (1991) – Stone (2000) time-dependent Lm[b] [a]	Lifton et al. (2014) LSD[c] [a]
13T4a	1840 ± 340 (370)	2160 ± 450 (490)
13T4b	2860 ± 320 (390)	3360 ± 380 (460)
13T5	2600 ± 240 (300)	2930 ± 270 (360)
13T15	11200 ± 700 (1100)	12900 ± 740 (1300)

[a] The ^{10}Be exposure ages were calculated with the CRONUScalc online calculator (http://web1.ittc.ku.edu:8888/2.0; version 2.0; Marrero et al., 2016) using two different scaling models. The internal errors of the exposure ages are based on the analytical uncertainty only. The total uncertainties provided by CRONUScalc also include the uncertainty of the local ^{10}Be production rate and are given in parentheses (Marrero et al., 2016; Phillips et al., 2016). The 2.7% error of the secondary AMS standard S2007N relative to the primary standard ICN-01-5-1 (Kubik and Christl, 2010) is not included in these uncertainties.

[b] The Lal (1991) – Stone (2000) time-dependent scaling model is referred to as the “Lm model” in section 5 and the CRONUScalc online calculator.

[c] The time-dependent scaling model of Lifton et al. (2014) is referred to as “LSD model” in section 5. The LSD scaling model has the abbreviation “Sf” in CRONUScalc (Marrero et al., 2016).

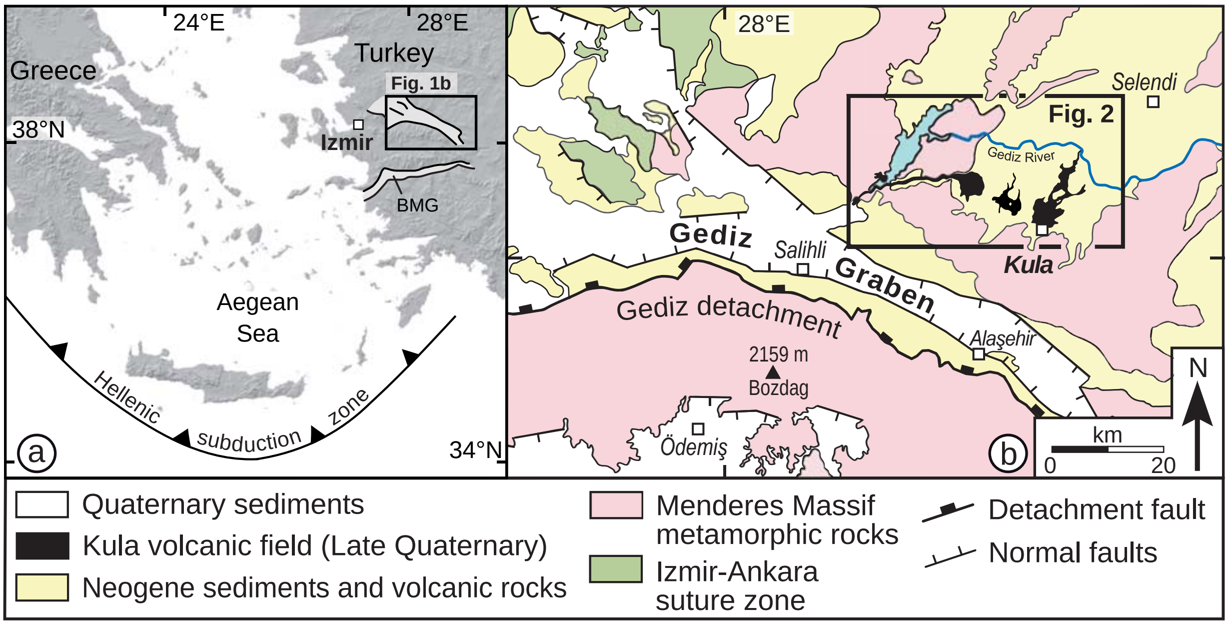

Heineke et al., Fig. 1

Fig. 1. (a) Map of the Aegean region – including Western Turkey – located in the back-arc of the Hellenic subduction zone. Black rectangle indicates the area shown in Fig. 1b. BMG denotes the Büyük Menderes graben. **(b)** Map showing the location of the Kula volcanic field north of the Gediz graben. Black rectangle indicates the area shown in Fig. 2.

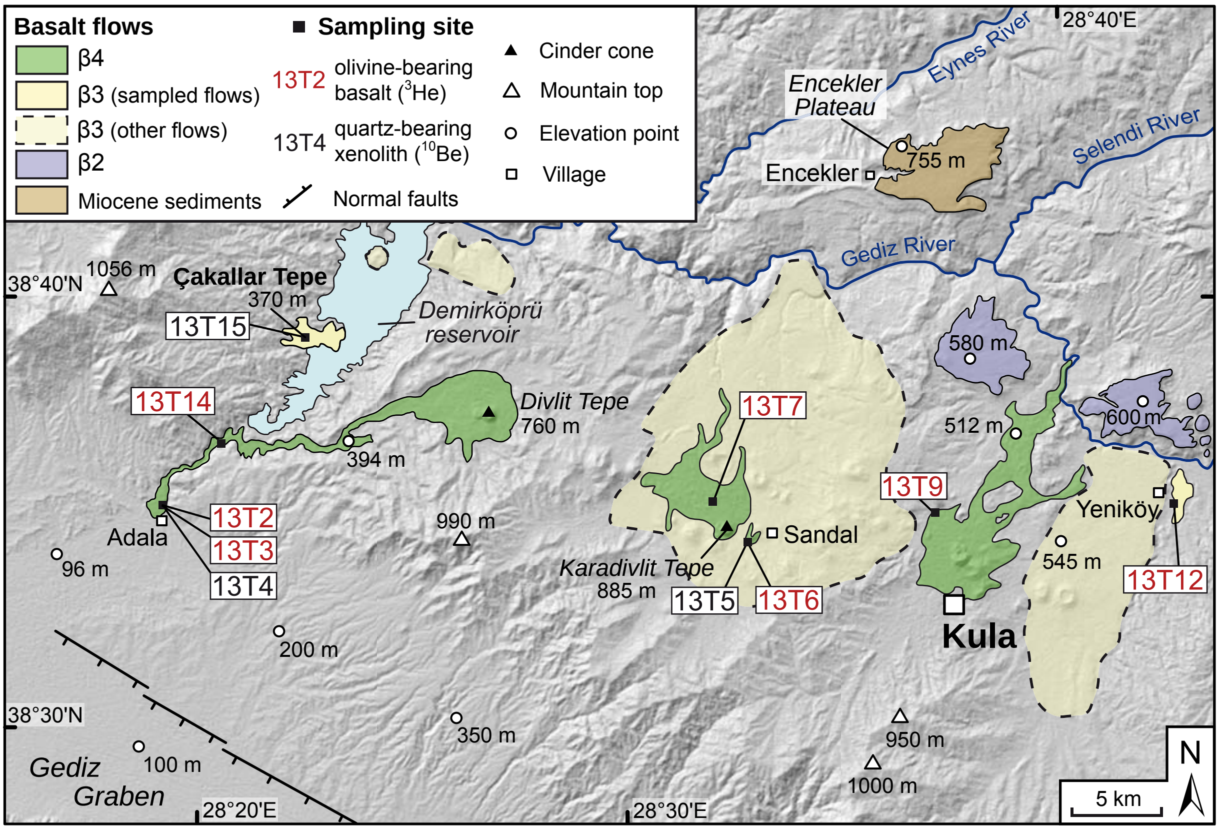

Heineke et al., Fig. 2

Fig. 2. Shaded relief image of the Kula volcanic field with sampling locations. The lava flows and cinder cones comprise three eruption phases, β2 to β4. With the exception of one sample from Çakallar Tepe and a sample from a β3 basalt flow near Yeniköy, all samples were collected from β4 flows and cinder cones. Lava flows belonging to the oldest β2 group form plateaus that have been incised by the Gediz River and its tributaries.

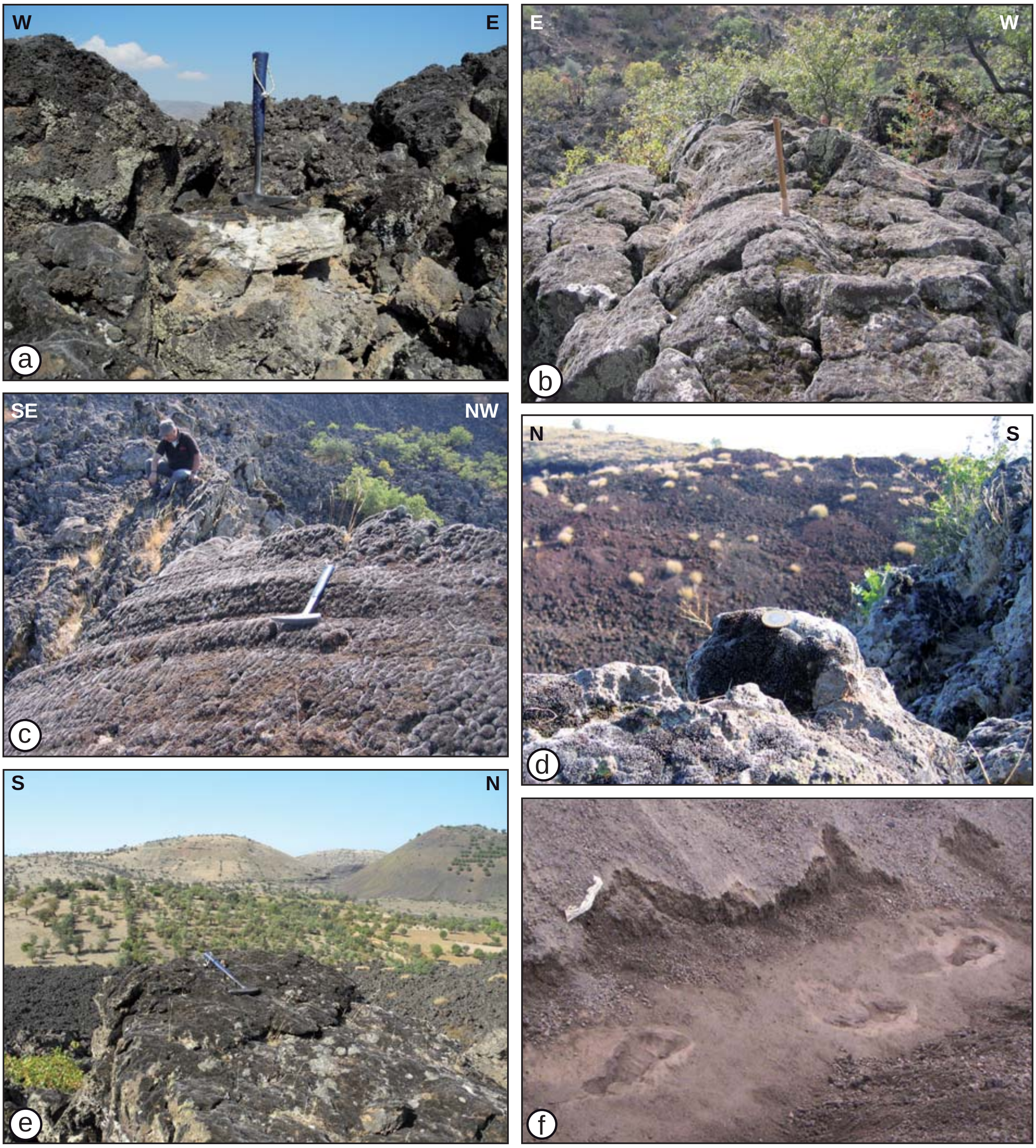

Heineke et al., Fig. 3

Fig. 3. Photographs of some of the sampling sites and samples (for locations see Fig. 2). **(a)** Angular augen gneiss xenolith (sample 13T4) at the surface of a 15-km-long block lava flow in the western part of the volcanic field. **(b)** Smooth, moss-covered surface of the same flow at the sampling site of 13T14. Note the preservation of the wavy surface texture, which indicates that erosion is negligible. **(c)** Well preserved flow feature indicating negligible surface erosion at the sampling site of 13T7. Note that the sampled surface is covered by a thin veneer of gray moss. **(d)** Sample 13T5 is a rounded metasedimentary xenolith found at the top of a cinder cone west of Sandal village. The moss-covered xenolith was firmly cemented to the tuff deposits underneath. **(e)** Large basalt block on the upper slope of the cone near Sandal village. Sample 13T6 was collected from the dark, moss-covered surface beneath the hammer. The lighter color of the surface in the foreground (which is overcast by a thinner coating of light-green lichen and dark moss) provides evidence for minor spallation at this part. **(f)** Fossil human footprints in volcanic ash deposits ~500 m west of the Çakallar Tepe cinder cone. Photograph courtesy of the Kula Municipality.

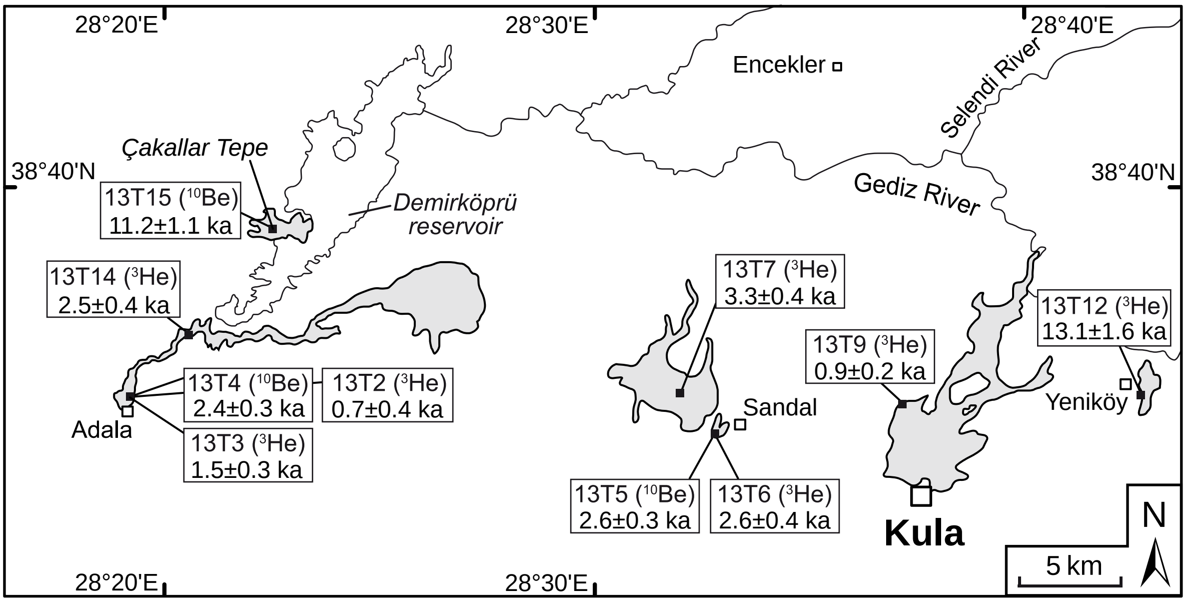

Heineke et al., Fig. 4

Fig. 4. Simplified map of the Kula volcanic field with sampling locations and ^{3}He and ^{10}Be exposure ages. All lava flows and cinder cones sampled are indicated in gray.